Letter

# Particle-resolved study of the onset of turbulence

E. Joshi [1,*] M. H. Thoma [2] and M. Schwabe [3]

[1]*Institut für Materialphysik im Weltraum, Deutsches Zentrum für Luft- und Raumfahrt (DLR), 51147 Köln, Germany*

[2]*I. Physikalisches Institut, Justus-Liebig Universität Gießen, 35392 Gießen, Germany*

[3]*Deutsches Zentrum für Luft- und Raumfahrt (DLR), Institut für Physik der Atmosphäre, 82234 Oberpfaffenhofen, Germany*

(Received 13 June 2023; accepted 13 October 2023; published 18 January 2024)

The transition from laminar to turbulent flow is an immensely important topic that is still being studied. Here we show that complex plasmas, i.e., microparticles immersed in a low temperature plasma, make it possible to study the particle-resolved onset of turbulence under the influence of damping, a feat not possible with conventional systems. We performed three-dimensional (3D) molecular dynamics (MD) simulations of complex plasmas flowing past an obstacle and observed 3D turbulence in the wake and forewake region of this obstacle. We found that we could reliably trigger the onset of turbulence by changing key parameters such as the flow speed and particle charge, which can be controlled in experiments, and show that the transition to turbulence follows the conventional pathway involving the intermittent emergence of turbulent puffs. The power spectra for fully developed turbulence in our simulations followed the $-5/3$ power law of Kolmogorovian turbulence in both time and space. We demonstrate that turbulence in simulations with damping occurs after the formation of shock fronts, such as bow shocks and Mach cones. By reducing the strength of damping in the simulations, we could trigger a transition to turbulence in an undamped system. This work opens the pathway to detailed experimental and simulation studies of the onset of turbulence on the level of the carriers of the turbulent interactions, i.e., the microparticles.

DOI: 10.1103/PhysRevResearch.6.L012013

One of the oldest unsolved problems in physics is the problem of the onset of turbulence. The transition of a fluid from smooth, deterministic, "laminar" sheets of flow to a chaotic, disordered, "turbulent" flow with vortices and eddies has been studied extensively in various systems such as water [1,2], air [3], as well as plasmas [4–9], and yet the ability to predict the onset of turbulence remains poor. A common way to trigger turbulence in experiments and simulations is to study flow past an obstacle [10–13], as seen, for example, in Fig. 1. Most investigations of flow past an obstacle focus on the wake region [14–16], with little emphasis on the forewake region [17,18].

There is no generally agreed upon definition of turbulence [19], rather only signatures of dynamic behavior that are widely recognized to be associated with it [20]. Turbulent flows are [21] as follows:

(i) *Rotational*. Turbulence is accompanied by vortices and nonzero angular momentum.

(ii) *Chaotic*. Turbulence is characterized by irregularities in the flow in the form of rapid changes in velocity vectors, temperature, pressure, density, etc. The flow is disordered, and changes in the flow profile are intermittent, abrupt, and unpredictable.

(iii) *Diffusive*. The rate of mixing in fluids is higher when the flow is turbulent, especially in the direction perpendicular to the flow.

(iv) *Resistive*. Turbulence creates drag. Flow resistance increases in turbulent flows compared to that of laminar flow.

(v) *Self-similar*. Kolmogorov showed in 1941 that large vortices transfer energy into smaller vortices in an energy cascade until the energy is dissipated through molecular diffusion and viscosity [22,23]. The power spectra of energy cascades follow the power law $E(k) \propto k^n$, where $k$ is the wave number representing length scales. The equivalent power law $E(f) \propto f^n$ is true for the energy cascade in time, where $f$ represents frequency. For fully developed isotropic turbulence, $n = -5/3$ [24].

The main parameter characterizing turbulent flow is the Reynolds number, $\Re = vL/\nu$, where v, $L$, and $\nu$ represent the characteristic flow speed, characteristic length scale, and kinematic viscosity, respectively. In this work, we use the bulk flow speed and the size of the cavity created by the obstacle for v and $L$, respectively. Generally, the transition from laminar flow to turbulent flow requires very high Reynolds numbers $\Re \geqslant O(1000)$ [25,26], however, low-$\Re$ turbulence has also been observed in many systems [27,28]. Studying low Reynolds number turbulence is important for fluids in biological systems and active matter, for instance, the flow of blood in vessels [29], or active swimmers such as bacteria [30], as well as highly viscous polymer flows in the case of elastic turbulence [31].

*eshita.joshi@dlr.de

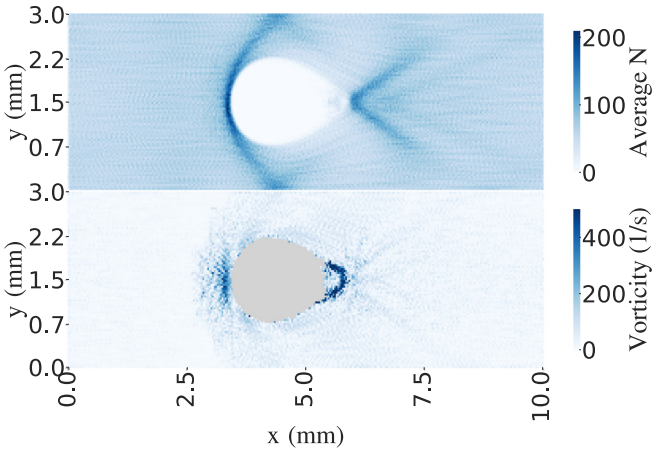


FIG. 1. An example turbulent simulation with particles flowing from the left to the right seen in a slice of position $z = (1.9$ to $2.1)$ mm. (top) Number of particles, and (bottom) $z$ vorticity component are averaged in bins of size $0.03 \times 0.03 \times 0.2\,\mathrm{mm}^3$ over 1 s. The empty pixels are colored in gray to mark the obstacle and the cavity around it. Turbulence can be seen in the forewake region in front of the bow shock, and in the wake region near the Mach cones.

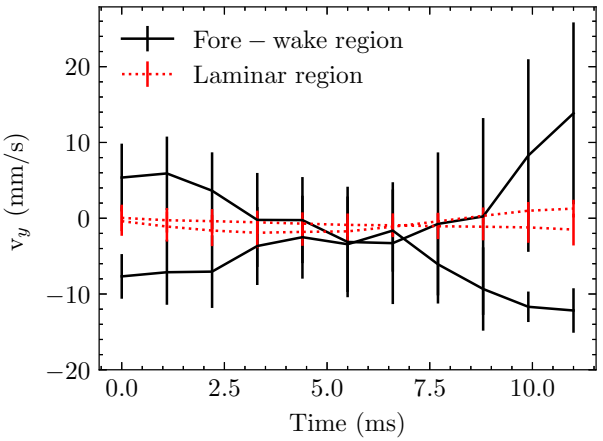


FIG. 2. Plot of the mean and standard error of the flow velocity $v_y$ (perpendicular to the bulk flow direction) of two sets of five randomly chosen particles within the laminar (red dotted lines) and forewake (black solid lines) region. In the laminar region, particle velocities $v_y$ have little fluctuations over time implying a regular and ordered flow with almost no fluid mixing. On the other hand, $v_y$ in the forewake region shows large random fluctuations on very short timescales, characteristic of intermittency. This indicates an irregular and disordered flow state with increased fluid mixing.

One such system with very low Reynolds number values, $\Re \sim O(10)$, is a complex plasma. Complex plasmas are low-pressure and temperature plasmas with micrometer-sized particles embedded in them [32]. These particles collect charges on their surfaces to become highly negatively charged, and as a result can become strongly coupled. Experiments are typically performed at pressures of the background gas of the order of (1–50) Pa, which means that the microparticle dynamics are not over damped as in colloids [33], but the Epstein damping force resulting from friction with the background gas is nevertheless an important force acting on the microparticles [34]. Turbulence in complex plasmas has been primarily studied in the context of experiments on waves [35–40] and simulations of fully developed turbulence [41], or 2D turbulence [42,43]. The plasma is treated as background since it is the motion of the microparticles that becomes turbulent and not the motion of the plasma. In this work, we discuss the turbulence forming inside the microparticle system and compare it with general fluid turbulence. Studying turbulence in complex plasmas has the advantage that each microparticle is large enough to be imaged directly, allowing for particle-resolved studies [44]. This will help understand the onset of turbulence in more detail, and to eventually develop methods to better control it.

In this Letter, we demonstrate how complex plasmas can be used to study the onset of turbulence in detail. For this, we performed 3D molecular dynamics (MD) simulations of subsonic and supersonic complex plasma flow past an obstacle with turbulence in the wake and forewake regions. We will first present an example of a turbulent simulation and show that it is consistent with the hallmarks of turbulence listed above. We will then discuss the transition of laminar flow to turbulent flow, as well as the transition from turbulence in a damped to an undamped system as observed in our simulations. We found that we can reliably trigger the onset of turbulence by changing the flow speed and particle charge.

We used the open source software "Large-scale Atomic/Molecular Massively Parallel Simulator" (LAMMPS) [45,46] to generate the simulations. As an MD simulator, LAMMPS only simulates the microparticle motion and not the background plasma. We typically used a time step of 0.1 ms and a data acquisition rate of 1000 fps, and a simulation box with dimensions $10 \times 3 \times 3\,\mathrm{mm}^3$ with periodic boundary conditions. The data acquisition rate was changed to 10 000 fps to generate the power spectra in time given in Fig. 3. We simulated microparticles as point charges with an equilibrium average interparticle distance of 150 μm with a Yukawa interparticle potential. The particle charge used was $q = -3481$ e (elementary charges) and the Debye length was $\lambda_D = 100$ μm [41]. The mass of the point charges was set to $3 \times 10^{-14}$ kg, mimicking microparticles with mass density $\rho = 1510\,\mathrm{kg/m}^3$ and diameter $d = 3.38\,\mu\mathrm{m}$. We used a Langevin dynamics thermostat [47] with an Epstein damping coefficient [34] corresponding to argon gas at a temperature and pressure of 2000 K and 10 Pa, respectively. The thermostat temperature was high in order to obtain a fluid ensemble of microparticles at the given pressure. The main forces acting on the particles in the simulation are, therefore, the interparticle force given by the Yukawa potential, the Langevin force due to the thermostat, and the Epstein damping due to the friction with the background gas.

We included the obstacle using a point charge of $-3 \times 10^7$ e with a fixed position at the coordinates $(x, y, z) = (4.5, 1.5, 2.0)$ mm. As observed in experiments [48–50], this high negative charge repelled the microparticles and thus resulted in a cavity around the point charge. In simulations in which the particles at a thermostat temperature of 2000 K were stationary, the cavity was spherical with a diameter of 1.4 mm. Please note that due to the periodic boundary conditions used in all dimensions, the simulation actually consisted of an infinite grid of obstacles. Increasing the size of the

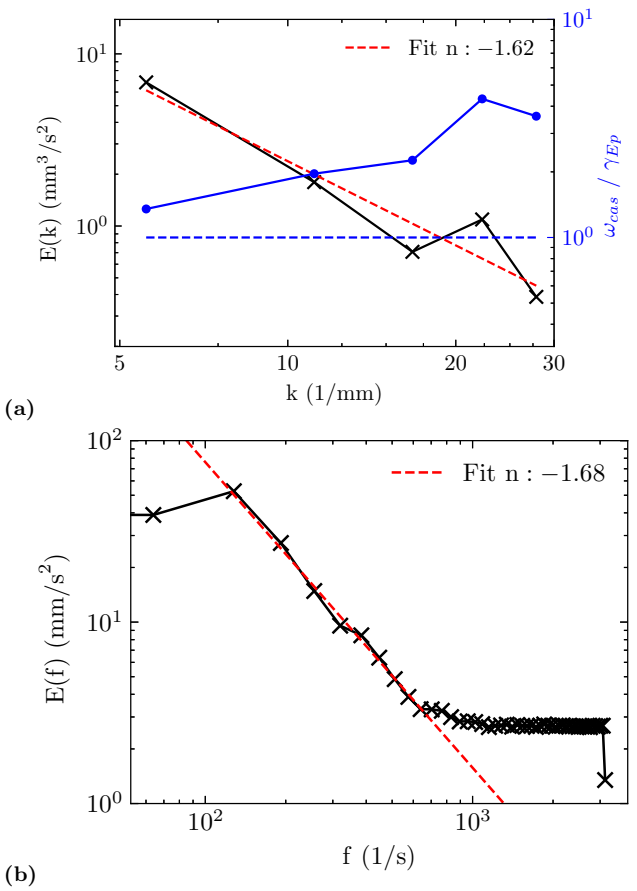


FIG. 3. Power spectra in (a) space and (b) time corresponding to the simulation in Fig. 1. Power spectra are shown from the interparticle distance to the size of the turbulent region in space, and till the Nyquist frequency of 5000 Hz in time. Both subplots show approximately the $n = -5/3$ power law characteristic of turbulent flows. The cascade rate $\omega_{\text{cas}}$ is greater than the damping rate $\gamma_{\text{Ep}}$, showing that the system was in the regime where turbulence could develop. The red dashed lines show the linear fit through the data, whereas the horizontal blue dashed line shows where $\omega_{\text{cas}} = \gamma_{\text{Ep}}$.

simulation box to ensure that the disturbed flow from one obstacle did not interfere with that around another obstacle showed no changes to our results.

We created a flow of particles past the obstacle by applying a constant force $F_{\text{ext}} = 10^{-11} - 10^{-13}$ N in the $x$ direction to the microparticles, depending on the desired bulk flow speed. An external force of $F_{\text{ext}} = 10^{-13}$ N could be produced in experiments by an electric field with a magnitude of 180 V/m. Due to the damping force, this resulted in a steady flow from the left to the right of the simulation box with periodic boundary conditions. The simulation box was large enough along $x$ for the particle motion to return to laminar before reaching the boundaries of the box. The main parameter used to characterize the flow at speed v is the Mach number, $\mathcal{M} = \text{v}/C_s$, where $C_s = \sqrt{Z_d k_B T_i / m_d}$ is the speed of sound in the system [51], with $T_i$ as the thermostat temperature, $m_d$ as the microparticle mass, and $Z_d = q/e$. For supersonic velocity, $\mathcal{M} > 1$.

Previous studies of supersonic flow have reported turbulence as well as Mach cones in the wake of an obstacle [52–56]. However, there have been few investigations of forewake turbulence or on the importance of shock fronts in triggering the onset of turbulence in damped systems. Hence, we will be focusing on forewake turbulence in this work. An example of wake and forewake turbulence in our simulation is provided in Fig. 1, with an accompanying movie in the Supplemental Material [57]. This is a 2D slice of the simulation box which shows the spatial distribution of vorticity $\omega_z = \frac{\partial \text{v}_y}{\partial x} - \frac{\partial \text{v}_x}{\partial y}$ around the obstacle averaged over one second of simulation time with a bin size of $0.03 \times 0.03 \times 0.2\,\text{mm}^3$. The vorticity per bin was calculated by averaging the difference in $\text{v}_x$ and $\text{v}_y$ across neighboring horizontal and vertical bins, respectively. Shock fronts such as Mach cones and a bow shock can be seen in Fig. 1 (top). Figure 1 (bottom) shows that vortices were generated in two main regions. The first is the wake of the obstacle, where the particles deflected by the obstacle flowed into the Mach cone. The second is the fore-wake region of the obstacle, where the incoming particles flowed into the bow shock. In both cases, vorticies were induced when particles flowed directly into a shock front. This observation is similar to the experimental observation of turbulence in Ref. [44], where the flow of particles directly into a dust-acoustic wavefront induced turbulence. The existence of vortices in the wake and forewake regions of the simulation satisfies condition i of the hallmarks of turbulence.

In the following, we study the flow in two regions in detail, a laminar region with position $0 \leqslant x \leqslant 1$ mm, $1 \leqslant y \leqslant 2$ mm, and $1 \leqslant z \leqslant 2$ mm; and a turbulent region corresponding to the forewake with position $2.5 \leqslant x \leqslant 3.5$ mm, $0.8 \leqslant y \leqslant 2.2$ mm, and $0.8 \leqslant z \leqslant 2.2$ mm. The evolution of the particle velocities perpendicular to the flow direction is given in Fig. 2. The particle motion in the laminar flow was smooth, ordered, and predictable, with almost no fluid mixing perpendicular to the flow direction. In contrast, the particle motion in the forewake was unpredictable and disordered, with irregularities in the flow and abrupt changes in the velocity. This is an example of intermittency in fully developed turbulence where the kinetic energy (and hence velocity) undergoes abrupt changes in a short time [24,58]. There was also increased mixing of the fluid in the turbulent region, especially in the direction perpendicular to the flow, as seen by the increased magnitude of $\text{v}_y$. This satisfies conditions ii and iii listed above.

The driving force causing the particles to flow from the left to the right of the simulation box was applied uniformly. The normalized kinetic energy, $(\text{ke}-\mu_{\text{ke}})/\sigma_{\text{ke}}$, of the particles in the laminar and chaotic regions of the forewake, where $\mu_{\text{ke}}$ and $\sigma_{\text{ke}}$ are the mean and standard deviation of the particle kinetic energy at a given time, is plotted in Fig. S1 in the Supplemental Material [57]. It shows that the kinetic energy of the chaotic region was significantly lower than that of the laminar flow for the same driving force. This indicates an increased flow resistance in the forewake region, satisfying condition iv of the hallmarks of turbulence.

To separate the kinetic energy due to the driving force and that due to the turbulent interparticle interactions, we define turbulent velocity $\mathbf{v}'$ and turbulent kinetic energy TKE as

$$\mathbf{v}' = \mathbf{v} - \bar{\mathbf{v}} \quad \text{and} \quad \text{TKE} = \tfrac{1}{2} m \text{v}'^2, \tag{1}$$

where $\bar{\mathbf{v}}$ is the local Reynolds-averaged flow velocity calculated with 3D bins of size $(250\,\mu\text{m})^3$ averaged over one second, and $m$ denotes the particle mass. We used $\mathbf{v}'$ to calculate the power spectra in space, and $\mathbf{v}$ to calculate the spectra in time.

The transfer of turbulent kinetic energy from large scales to smaller scales in 3D turbulence follows a power law distribution of $E(k) \propto k^n$ with $\mathrm{n} = -5/3$, as first described by Kolmogorov [22,23]. The one-dimensional power spectra in $x$, $y$, and $z$ are plotted in Fig. S2 in the Supplemental Material [57]. They all show the $\mathrm{n} = -5/3$ power law, showing that turbulence is three-dimensional and isotropic in our system [24]. The power spectra in time and 3D space are given in Fig. 3, which also reflect the $\mathrm{n} = -5/3$ power law, further satisfying condition v of the signatures of turbulence. The power spectra were calculated using the Wiener-Khintchine theorem [59,60], which states that the power spectrum is the Fourier transform of the velocity correlation function. This is given by the relation

$$E(f) = \frac{1}{2\pi}\int_{-\infty}^{+\infty} e^{ifs}\Gamma(s)ds, \quad \text{and} \tag{2}$$

$$E(k) = \frac{1}{2\pi}\int_{-\infty}^{+\infty} e^{ikx}\langle \mathrm{v}(0)\mathrm{v}(x)\rangle dx, \tag{3}$$

where $\Gamma(s) = \langle \mathrm{v}(t)\mathrm{v}(t')\rangle$ is the velocity correlation function averaged over all particles, and $s = |t - t'|$. The power spectra follow the $\mathrm{n} = -5/3$ law from $\mathrm{f} \sim 110\,\mathrm{Hz}$ to $\mathrm{f} \sim 660\,\mathrm{Hz}$, and from spatial scales of roughly 225 μm to 1.14 mm. These values are consistent with the estimated Kolmogorov microscales [24,61]. The Kolmogorov dissipation length ($\eta \sim 230\,\mu\text{m}$) and time ($1/\tau_n \sim 80$ Hz) were calculated using the mean rate of kinetic energy transfer, $\varepsilon$, and the local viscosity, $\nu$. The local viscosity, $\nu = \frac{1}{3}vl$ was estimated using the average interparticle distance as the mean-free path, $l$, as well as the locally averaged velocity, $v$. On the other hand, $\varepsilon$ was determined numerically using $\frac{1}{2}\frac{\partial\langle \mathrm{v}^2\rangle}{\partial t}$. It can also be seen in Fig. 3 that the rate of energy cascade, $\omega_{\mathrm{cas}} = k\sqrt{2kE(k)}$, is greater than the rate of damping, $\gamma_{Ep} = 36\ \mathrm{s}^{-1}$, given by the Epstein damping coefficient [34], for all considered wave numbers. This shows that our system was in the regime where vortices could transfer energy from larger length scales to smaller scales without dissipation until the cascade reached interparticle distances [44]. The five conditions representing the hallmarks of turbulence listed above, plus one specific for damped systems, are thus shown to be satisfied.

In the following, we will discuss a series of simulations studying the onset of turbulence. The onset of this turbulent flow in the simulations was triggered by changing one of two main parameters: the flow speed and the particle charge. Changing the flow speed changed $\mathcal{M}$ and $\Re$. Changing the particle charge affected viscosity, and hence $\Re$, but also the speed of sound $C_s = \sqrt{Z_d k_B T_i/m_d}$ and hence, $\mathcal{M}$. The Mach number varied from 0 to 2 and the Reynolds number ranged from 2 to 50. Increasing $\mathcal{M}$ led to the formation of shock fronts, such as Mach cones and bow shocks. These shock fronts were crucial for triggering the onset of turbulence in our simulations. In the simulations with damping, no turbulence was observed in the forewake without the presence of shock fronts, even with particles flowing around the obstacle at supersonic speeds. In the forewake region, the laminar flow of particles flowing directly perpendicular into the bow shock triggered the flow to become turbulent. Similarly, particles accelerated by the obstacle from above and below that flowed directly into the Mach cone in the wake became turbulent. The significance of the presence of bow shocks and Mach cones can be seen in Fig. 4, which plots the slope of the power spectra (normalized by $-5/3$) as a function of average flow speed for three different particle charges for otherwise identical conditions. The vertical dashed lines mark the speed where the flow becomes supersonic, with colors corresponding to the three simulated cases of particle charge. It can be seen clearly that the normalized slope reaches a value of one only after the flow becomes supersonic.

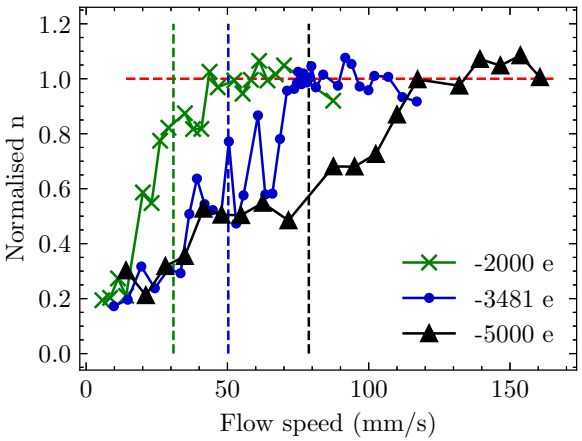


FIG. 4. Dependence of the power spectrum slopes normalized by $-5/3$, obtained via a linear fit in the region 100 Hz < f < 700 Hz of the power spectra in time, on the flow speed and the particle charge. Vertical lines indicate the speed of sound for the corresponding particle charge determined numerically from the Mach cone opening angle.

The shape of the plots can be explained by the following. For a given supersonic flow speed, the onset of turbulence could be triggered by decreasing the viscosity, and hence, increasing $\Re$. This was achieved by decreasing the magnitude of the particle charge and keeping all other parameters constant. If $\Re$ is high enough for turbulence to develop, for instance for a particle charge of $-2000$ e, $\Re \sim O(10)$, then the flow becomes turbulent as soon as $\mathcal{M} > 1$. If $\Re$ is low, for instance for a particle charge of $-5000$ e, $\Re \sim O(1)$, then upon reaching $\mathcal{M} > 1$ no turbulence develops. $\Re$ increases linearly with increasing flow speed until it is high enough for turbulence to develop. For higher particle charges, $\Re$ is lower and thus the system requires higher $\mathcal{M}$ to become turbulent.

For supersonic flow velocities during the transition to turbulence, intermittent switching between laminar and turbulent regions was also observed. This is shown in Fig. 5. The flow in the forewake region was observed to switch from laminar to turbulent and back to laminar as transient turbulent puffs were created over time. This is characteristic of intermittent turbulence occurring during the transition to turbulence [42,62]. Animations of vorticity over time showing intermittent turbulence can be found in the Supplemental Material [57].

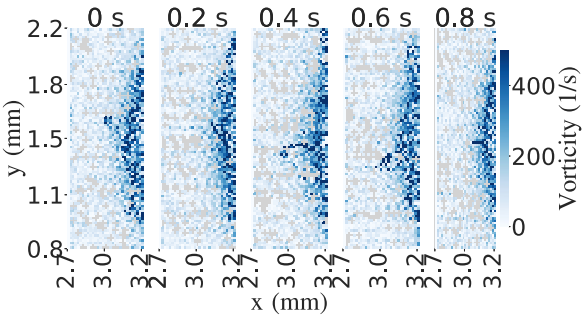


FIG. 5. Vorticity heatmap showing intermittent switching between laminar and turbulent regions as transient turbulent puffs form and decay over space and time.

The result that the formation of shock fronts is necessary for turbulence to develop is due to the presence of damping in typical conditions for complex plasma experiments that informed our simulations. To confirm this, we performed 3D simulations in a practically undamped system with supersonic flow, with a pressure corresponding to $10^{-5}$ Pa, and repeated the same analysis steps as before. The criteria for turbulence listed above were satisfied, and we observed turbulence in the undamped simulations even without the presence of shock fronts. The results of this analysis can be found in Figs. S3–S6 in the Supplemental Material [57].

To summarize, we report the results of 3D molecular dynamics simulations of a complex plasma with turbulent flow in the wake and forewake region of a supersonic obstacle. We confirmed that the flow indeed was turbulent by going through a checklist of the hallmarks of turbulence. Despite the microparticles being charged, so far we hypothesize that the turbulence displayed is characteristically similar to general fluid turbulence instead of plasma turbulence. A future study could explore the dependence on the interparticle potential of the characteristics of turbulence observed. We studied the onset of turbulence in multiple simulations and found that we could reliably trigger the onset of turbulence by changing parameters such as flow speed and particle charge. Turbulence was observed in the simulations with damping if and only if there was a flow of particles directly toward a shock front. We observed no turbulence in the absence of bow shocks and Mach cones. We demonstrated a dependence of the power spectra of energy cascade on $\mathcal{M}$ and $\Re$ by studying their evolution with increasing flow speed and particle charge. Intermittency was observed both during the onset of turbulence (in the form of transient turbulent puffs) and in fully developed turbulence (in the form of rapid changes to velocity vectors). The flow speeds, particle charges, and pressure regime used in this study are obtainable with typical complex plasma experimental setups. Therefore, we expect that our study can be used to inform future experiments and open up new research avenues for detailed particle-resolved studies of the onset of turbulence using complex plasmas.

The authors gratefully acknowledge funding of this work in the framework of the Nachwuchsgruppenprogramm im DLR-Geschäftsbereich Raumfahrt. We would like to thank V. Nosenko, P. Bajaj, and A. Ivlev for helpful discussions and their valuable feedback, and H. Thomas and J. Klamt for careful reading of the manuscript and for helpful comments.

[1] S. Nazarenko and S. Lukaschuk, Wave turbulence as a part of general turbulence theory, Annu. Rev. Condens. Matter Phys. **7**, 61 (2016).
[2] E. Falcon and N. Mordant, Experiments in surface gravity-capillary wave turbulence, Annu. Rev. Fluid Mech. **54**, 1 (2022).
[3] N. E. Busch and H. A. Panofsky, Recent spectra of atmospheric turbulence, Q. J. R. Meteorol. Soc. **94**, 132 (1968).
[4] A. Vedenov, Theory of a weakly turbulent plasma, Rev. Plasma Phys. **3**, 229 (1967).
[5] V. N. Tsytovich and D. L. Burdick, *Theory of Turbulent Plasma* (Springer, 1977).
[6] Hasegawa and M. Wakatani, Plasma edge turbulence, Phys. Rev. Lett. **50**, 682 (1983).
[7] M. V. Goldman, Strong turbulence of plasma waves, Rev. Mod. Phys. **56**, 709 (1984).
[8] L. Comisso and L. Sironi, Ion and electron acceleration in fully kinetic plasma turbulence, Astrophys. J. Lett. **936**, L27 (2022).
[9] R. Marino and L. Sorriso-Valvo, Scaling laws for the energy transfer in space plasma turbulence, Phys. Rep. **1006**, 1 (2023).
[10] A. G. Tomboulides and S. A. Orszag, Numerical investigation of transitional and weak turbulent flow past a sphere, J. Fluid Mech. **416**, 45 (2000).
[11] H. Charan and R. Ganesh, Supersonic flows past an obstacle in Yukawa liquids, Phys. Plasmas **25**, 043706 (2018).
[12] J. L. Ortiz-Tarin, K. C. Chongsiripinyo, and S. Sarkar, Stratified flow past a prolate spheroid, Phys. Rev. Fluids **4**, 094803 (2019).
[13] P. Puthan, G. Pawlak, and S. Sarkar, Wake vortices and dissipation in a tidally modulated flow past a three-dimensional topography, J. Geophys. Res.: Oceans **127**, e2022JC018470 (2022).
[14] H. Zhang, U. Fey, B. R. Noack, M. König, and H. Eckelmann, On the transition of the cylinder wake, Phys. Fluids **7**, 779 (1995).
[15] S.-y. Wang, F.-b. Tian, L.-b. Jia, X.-y. Lu, and X.-z. Yin, Secondary vortex street in the wake of two tandem circular cylinders at low Reynolds number, Phys. Rev. E **81**, 036305 (2010).
[16] G. Y. Dynnikova, Y. A. Dynnikov, and S. V. Guvernyuk, Mechanism underlying Kármán vortex street breakdown preceding secondary vortex street formation, Phys. Fluids **28**, 054101 (2016).
[17] C. B. Haakonsen and I. H. Hutchinson, The electron forewake: Shadowing and drift-energization as flowing magnetized plasma encounters an obstacle, Phys. Plasmas **22**, 102103 (2015).
[18] S. K. Tiwari and A. Sen, Fore-wake excitations from moving charged objects in a complex plasma, Phys. Plasmas **23**, 100705 (2016).

[19] A. Groisman and V. Steinberg, Elastic turbulence in a polymer solution flow, Nature (London) **405**, 53 (2000).

[20] J. Mathieu and J. Scott, *An Introduction to Turbulent Flow* (Cambridge University Press, 2000).

[21] S. Nazarenko, Wave turbulence as a part of general turbulence theory, in *Wave Turbulence* (Springer Berlin Heidelberg, Berlin, Heidelberg, 2011), pp. 17–28.

[22] A. N. Kolmogorov, Equations of turbulent motion in an incompressible fluid, Proc. USSR Acad. Sci. **30**, 299 (1941).

[23] A. N. Kolmogorov, V. Levin, J. C. R. Hunt, O. M. Phillips, and D. Williams, Dissipation of energy in the locally isotropic turbulence, Proc. R. Soc. London A **434**, 15 (1991).

[24] U. Frisch, *Turbulence: The Legacy of A. N. Kolmogorov* (Cambridge University Press, 1995).

[25] B. Hof, C. W. H. van Doorne, J. Westerweel, and F. T. M. Nieuwstadt, Turbulence regeneration in pipe flow at moderate reynolds numbers, Phys. Rev. Lett. **95**, 214502 (2005).

[26] A. J. Smits, B. J. McKeon, and I. Marusic, High-reynolds number wall turbulence, Annu. Rev. Fluid Mech. **43**, 353 (2011).

[27] G. R. Wang, F. Yang, and W. Zhao, There can be turbulence in microfluidics at low Reynolds number, Lab Chip **14**, 1452 (2014).

[28] M. Linkmann, G. Boffetta, M. C. Marchetti, and B. Eckhardt, Phase transition to large scale coherent structures in two-dimensional active matter turbulence, Phys. Rev. Lett. **122**, 214503 (2019).

[29] F. Ghalichi, X. Deng, A. D. Champlain, Y. Douville, M. King, and R. Guidoin, Low Reynolds number turbulence modeling of blood flow in arterial stenoses, Biorheology **35**, 281 (1998).

[30] Y. Peng, Z. Liu, and X. Cheng, Imaging the emergence of bacterial turbulence: Phase diagram and transition kinetics, Sci. Adv. **7**, eabd1240 (2021).

[31] V. Steinberg, Elastic turbulence: An experimental view on inertialess random flow, Annu. Rev. Fluid Mech. **53**, 27 (2021).

[32] G. E. Morfill and A. V. Ivlev, Complex plasmas: An interdisciplinary research field, Rev. Mod. Phys. **81**, 1353 (2009).

[33] A. Ivlev, G. Morfill, H. Löwen, and P. C. Royall, *Complex Plasmas and Colloidal Dispersions: Particle-Resolved Studies of Classical Liquids and Solids* (World Scientific Publishing Company, 2012).

[34] P. S. Epstein, On the resistance experienced by spheres in their motion through gases, Phys. Rev. **23**, 710 (1924).

[35] J. Pramanik, B. Veeresha, G. Prasad, A. Sen, and P. Kaw, Experimental observation of dust-acoustic wave turbulence, Phys. Lett. A **312**, 84 (2003).

[36] Y.-Y. Tsai, M.-C. Chang, and L. I, Observation of multifractal intermittent dust-acoustic-wave turbulence, Phys. Rev. E **86**, 045402(R) (2012).

[37] J.-Y. Tsai, P.-C. Lin, and L. I, Single to multiple acoustic vortex excitations in the transition to defect-mediated dust acoustic wave turbulence, Phys. Rev. E **101**, 023210 (2020).

[38] S. Zhdanov, M. Schwabe, C. Räth, H. M. Thomas, and G. E. Morfill, Wave turbulence observed in an auto-oscillating complex (dusty) plasma, Europhys. Lett. **110**, 35001 (2015).

[39] M. Schwabe, S. Zhdanov, and C. Räth, Turbulence in an auto-oscillating complex plasma, IEEE Trans. Plasma Sci. **46**, 684 (2018).

[40] H.-W. Hu, Y.-C. Zhao, and I. Lin, Avalanche structural rearrangements in cold dusty plasma liquids through cascaded coherent excitations of heterogeneous multiscale thermal acoustic waves, Phys. Rev. Res. **4**, 023116 (2022).

[41] M. Schwabe, S. Zhdanov, C. Räth, D. B. Graves, H. M. Thomas, and G. E. Morfill, Collective effects in vortex movements in complex plasmas, Phys. Rev. Lett. **112**, 115002 (2014).

[42] G. Gogia, W. Yu, and J. C. Burton, Intermittent turbulence in a many-body system, Phys. Rev. Res. **2**, 023250 (2020).

[43] E. G. Kostadinova, R. Banka, J. L. Padgett, C. D. Liaw, L. S. Matthews, and T. W. Hyde, Fractional Laplacian spectral approach to turbulence in a dusty plasma monolayer, Phys. Plasmas **28**, 073705 (2021).

[44] P. Bajaj, A. Ivlev, C. Räth, and M. Schwabe, Studying turbulence in a fluid with background damping, Phys. Rev. E **107**, 064603 (2023).

[45] S. Plimpton, Fast parallel algorithms for short-range molecular dynamics, J. Comput. Phys. **117**, 1 (1995).

[46] A. P. Thompson, H. M. Aktulga, R. Berger, D. S. Bolintineanu, W. M. Brown, P. S. Crozier, P. J. in 't Veld, A. Kohlmeyer, S. G. Moore, T. D. Nguyen, R. Shan, M. J. Stevens, J. Tranchida, C. Trott, and S. J. Plimpton, LAMMPS - a flexible simulation tool for particle-based materials modeling at the atomic, meso, and continuum scales, Comput. Phys. Commun. **271**, 108171 (2022).

[47] T. Schneider and E. Stoll, Molecular-dynamics study of a three-dimensional one-component model for distortive phase transitions, Phys. Rev. B **17**, 1302 (1978).

[48] J. K. Meyer, R. L. Merlino, J. R. Heinrich, and S.-H. Kim, Flow of dusty plasma around an obstacle, IEEE Trans. Plasma Sci. **42**, 2690 (2014).

[49] S. Jaiswal, M. Schwabe, A. Sen, and P. Bandyopadhyay, Experimental investigation of dynamical structures formed due to a complex plasma flowing past an obstacle, Phys. Plasmas **25**, 093703 (2018).

[50] Y. Bailung, B. Chutia, T. Deka, A. Boruah, S. K. Sharma, S. Kumar, J. Chutia, Y. Nakamura, and H. Bailung, Vortex formation in a strongly coupled dusty plasma flow past an obstacle, Phys. Plasmas **27**, 123702 (2020).

[51] M. Schwabe, K. Jiang, S. Zhdanov, T. Hagl, P. Huber, A. V. Ivlev, A. M. Lipaev, V. I. Molotkov, V. N. Naumkin, K. R. Sütterlin, H. M. Thomas, V. E. Fortov, G. E. Morfill, A. Skvortsov, and S. Volkov, Direct measurement of the speed of sound in a complex plasma under microgravity conditions, Europhys. Lett. **96**, 55001 (2011).

[52] D. Samsonov, J. Goree, Z. W. Ma, A. Bhattacharjee, H. M. Thomas, and G. E. Morfill, Mach cones in a coulomb lattice and a dusty plasma, Phys. Rev. Lett. **83**, 3649 (1999).

[53] A. Melzer, S. Nunomura, D. Samsonov, Z. W. Ma, and J. Goree, Laser-excited Mach cones in a dusty plasma crystal, Phys. Rev. E **62**, 4162 (2000).

[54] G. E. Morfill, M. Rubin-Zuzic, H. Rothermel, A. V. Ivlev, B. A. Klumov, H. M. Thomas, U. Konopka, and V. Steinberg, Highly resolved fluid flows: "Liquid plasmas" at the kinetic level, Phys. Rev. Lett. **92**, 175004 (2004).

[55] K. Jiang, V. Nosenko, Y. F. Li, M. Schwabe, U. Konopka, A. V. Ivlev, V. E. Fortov, V. I. Molotkov, A. M. Lipaev, O. F. Petrov, M. V. Turin, H. M. Thomas, and G. E. Morfill, Mach cones in a

three-dimensional complex plasma, Europhys. Lett. **85**, 45002 (2009).

[56] H. Charan and R. Ganesh, Molecular dynamics study of flow past an obstacle in strongly coupled Yukawa liquid, Phys. Plasmas **23**, 123703 (2016).

[57] See Supplemental Material at http://link.aps.org/supplemental/10.1103/PhysRevResearch.6.L012013 for additional information, plots, and animations.

[58] T. A. Carter, Intermittent turbulence and turbulent structures in a linear magnetized plasma, Phys. Plasmas **13**, 010701 (2006).

[59] N. Wiener, Generalized harmonic analysis, Acta Math. **55**, 117 (1930).

[60] A. Khintchine, Korrelationstheorie der stationären stochastischen Prozesse, Math. Ann. **109**, 604 (1934).

[61] M. T. Landahl and E. Mollo-Christensen, *Turbulence and Random Processes in Fluid Mechanics*, 2nd ed. (Cambridge University Press, 1992).

[62] B. Eckhardt, T. M. Schneider, B. Hof, and J. Westerweel, Turbulence transition in pipe flow, Annu. Rev. Fluid Mech. **39**, 447 (2007).